The Advantages of Using an Electrochemical Quartz Nanobalance to Study the Electrochemical Conversions of Solid Microparticles

G. Inzelt* **and A. Róka**
Eötvös Loránd University, Institute of Chemistry,
Budapest, Pázmány Péter sétány 1/a, H-1117, Hungary

Original scientific paper
Received: July 21, 2008
Accepted: August 12, 2008

This paper discusses the importance of and opportunities for applying piezoelectric nanogravimetry in the investigation of immobilized microcrystals on electrodes. The selected experimental results presented shed light on the complex nature of the processes occurring in these systems. The problem of the first cycle or break-in effect is emphasized.

Key words:
Microcrystals, solid state voltammetry, electrochemical quartz crystal nanobalance, phenazine, tetracyanoquinodimethane, $Ru(III)Cl_3$, carbazole

Introduction

The investigation of particles and droplets immobilized on electrode surface has become an interesting and important field of electrochemistry.[1–38] It has proven useful in solving both fundamental and applied issues, e.g. determination of thermodynamic data of solid compounds, elucidation of solid-to-solid electrochemical reactions accompanied by phase transitions, qualitative and quantitative determination of the composition of different solid materials including alloys, mixtures of inorganic compounds (such as minerals, archaeological ceramic glazes), organic and organometallic compounds, or gaining a deeper understanding of insertion reactions.[1–4]

The method of voltammetry of immobilized microparticles[1–4] in combination with electrochemical nanogravimetry by using quartz crystal nanobalance (EQCN) – also called microbalance, and abbreviated as EQCM – is especially useful for the characterization of microcrystals attached to an electrode surface.[1–4,17,29,31–38] Although the cyclic voltammetry supplies information regarding the redox reactions occurring in these systems, the elucidation of the voltammograms is a very difficult, often impossible task without additional data concerning the sorption/desorption of ionic species and neutral molecules as well as dissolution and deposition processes. A unique opportunity is the investigation of the solid-solid phase transition. In order to demonstrate the importance of the application of this combined technique, the results obtained for phenazine,[33] tetracyanoquinodimethane,[37] α-$RuCl_3$[34,35] and carbazole[31] microcrystals will be presented. Usually the 'stabilized responses' are studied, however, in many cases the parent microcrystals undergo irreversible transformations during the first reduction-oxidation cycle. Therefore, it is also important to investigate this 'break-in' process which differs from that characteristic of conducting polymer films where usually only morphological changes occur. In this paper, the first-cycle or break-in phenomenon is emphasized.

Experimental

Phenazine (Aldrich), carbazole (Sigma), tetracyanoquinodimethane (EGA-Chemie), $RuCl_3$, $HClO_4$, $NaClO_4$, HCl, LiCl, NaCl, KCl, CsCl, and $HClO_4$ (Merck, analytical grade) were used as received. Double-distilled water was used. Ten and six MHz AT-cut crystals coated with gold were used in the EQCM measurements. The apparatus and its calibration were described in detail in our previous papers.[34–37] The geometrical and piezoelectrically active area of the working electrode (A) was 0.4 cm^2. A Pt wire was used as a counter electrode. The reference electrode was a sodium chloride saturated calomel electrode (SCE). All potentials are referred to SCE, E_{SCE} = 0.231 V vs. SHE.

The electrodes were prepared in two different ways. Usually the microcrystals were attached to the gold surface by wiping the electrode with a cotton swab or filter paper containing the material. Alternatively, in the case of phenazine, carbazole and tetracyanoquinodimethane (TCNQ), the electrodes were covered with the organic compounds by using the evaporation technique; i.e., the crystals were dissolved in tetrahydrofuran (THF) and some drops of the solution were placed on the electrode surface. (There was no difference regarding the behaviour

*Corresponding author: György Inzelt, e-mail: inzeltgy@chem.elte.hu

of the surface layers, i.e., the electrochemical responses were practically the same.)

Also proven is that there is no loss of material due to vibration of the oscillating quartz crystal.

Although the requirements (uniform and homogeneous surface layer) for applying the Sauerbrey equation[39] were not met perfectly, a rough estimation can be done based on the measured frequency values (Δf). The surface roughness effect – albeit the deposit cannot be considered as an ideally smooth and uniform layer – was ignored. The solution trapped within the surface features may influence the frequency response related to the surface mass changes. However, this effect causes an error no higher than 10 – 20 % in the mass calculated. The frequency-charge plots obtained were linear even at rather high frequency changes, i.e., for rather thick layers, which may indicate that the side effects are not substantial. Therefore, the Sauerbrey equation was used to calculate the surface mass changes (Δm) from the frequency changes (Δf), with an integral sensitivity [$C_f = (2.05 \pm 0.2) \cdot 10^8$ and $(0.85 \pm 0.2) \cdot 10^8$ Hz cm^2 g^{-1} for 10 MHz and 6 MHz crystals, respectively] that was determined in separate experiments.[32]

For the estimation of the apparent molar mass (M_{app}) of the incorporated species the following equation was used:

$$M_{app} = \frac{\Delta f\, A\, n\, F}{C_f Q} \qquad (1)$$

where Q is the charge consumed corresponding Δf, F is the Faraday constant, n is the number of electrons in the reaction.

The amount of immobilized material on the surface was estimated by measuring the crystal frequency before and after the deposition in dry state.

All solutions were purged with oxygen-free argon and an inert gas blanket was maintained throughout the experiments. The measurements were carried out at 25 °C.

An Elektroflex 453 potentiostat (Szeged) and a Philips universal frequency counter PM6685 connected with an IBM personal computer were used for control of the measurements and acquisition of data.

Results and discussion

Electrochemical transformations of α-$RuCl_3$

$RuCl_3$ is insoluble in water and organic solvents, which is associated with its polymeric structure in solid state. $RuCl_3$ microcrystals can be reduced and reoxidized in several steps in the presence of acidic and neutral aqueous solutions of different electrolytes. The results can be explained by the formation of complexes and intercalation compounds, which contain mixed valence Ru^{III}/Ru^{II}-centers, Cl^- ions, metals or H^+ ions, and solvent molecules, the ratio of which depends on the potential and the solution composition. The redox transformations also involve solid-state phase transitions.[34,35] The insertion of organic molecules (e.g., aniline or pyrrole) is also possible, and it results in polyaniline or polypyrrole – $RuCl_3$ nanocomposites.[36,38]

Figs. 1 and 2 show the cyclic voltammograms and the simultaneously detected EQCM frequency responses obtained for α-$RuCl_3$ microcrystals attached to a gold electrode in the presence of 5 mol dm^{-3} NaCl. Similar responses can be obtained in the presence of KCl, RbCl and CsCl, respectively, and also at different concentrations. For each system the first, 'break-in' cycle and the subsequent, 'stabilized' response are different. Furthermore, layers

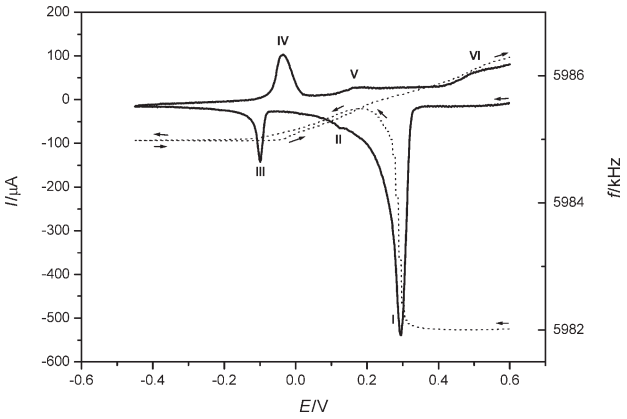

Fig. 1 – *Cyclic voltammograms (continuous line) and the simultaneously detected EQCM frequency responses (dotted line) for $RuCl_3$ microcrystals attached to a gold surface in the presence of 5 mol dm^{-3} solution of NaCl. Scan rate: 20 mV s^{-1}. First cycle.*

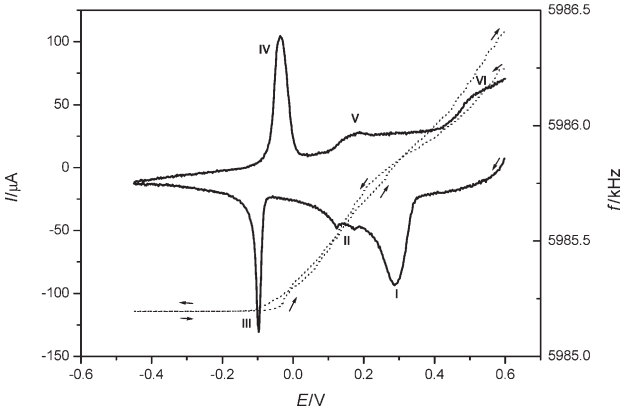

Fig. 2 – *Cyclic voltammograms (continuous line) and the simultaneously detected EQCM frequency responses (dotted line) for $RuCl_3$ microcrystals attached to a gold surface in the presence of 5 mol dm^{-3} solution of NaCl. Scan rate: 20 mV s^{-1}. Second cycle.*

of different thicknesses, i.e., different amounts of α-$RuCl_3$ on the gold surface have also been studied, in order to check the proportionality between the surface mass and the electrogravimetric (charge consumed and surface mass change) responses (Fig. 3).

During the first reduction step (peak I) the charge consumption is substantially higher than in the course of the further potential cycling, and the simultaneous rapid and intense mass decrease indicates that considerable chemical and structural transformations are occurring. Albeit a loss of the surface mass cannot be entirely excluded, the frequency increase is not related to the dissolution of the microcrystals, however, a large amount of water molecules and – to a much smaller extent – chloride ions – leave the crystal phase, forming in fact a new material that remains strongly attached to the gold or graphite surface. The extremely high frequency change at the first reduction process during the first cycle is related most likely to the stress effect originating from the phase transition of the surface layer and/or the removal of the water rigidly coupled to the surface into voids of the immobilized microcrystals. Depending on the amount of microcrystals on the electrode surface and the experimental conditions (the nature and concentration of the contacting electrolyte, scan rate and potential range) used after the 'break-in' cycle, stable electrochemical and nanogravimetric responses develop. The several reduction and reoxidation pairs of waves in the cyclic voltammograms and the simultaneous mass changes are in connection with the wide variety of intercalation reactions and complex formation during the electrochemical transformations. The mass change was reversible, in general during reduction mass increase, while during oxidation mass decrease occurred at medium electrolyte concentrations in three or more steps. The mass excursions are rather complicated involving different mass increase/decrease regions as a function of potential and the composition of the contacting solution.

Fig. 3 illustrates the effect of the amount of the deposited $RuCl_3$. Both the peak currents and the respective EQCM frequency changes at peak I during the first cycle are proportional to the dry thickness. The difference, i.e. the proportionality between the cyclic voltammetric peak currents as well as the frequency responses and the amount of material originally attached to the gold surface, is preserved even during the subsequent cycles. This may be interpreted as a combined effect of the desorption of the water molecules originally present in the crystal structure and the stress arising from the change in the crystal structure. At very thin layers (Fig. 3, curve 1), however, the first cycle effect is almost absent; therefore, it has to be assumed that the layers close to the metal surface have a different, probably more compact structure. These results reveal that the 'first cycle effect' is also associated with the removal of water that is elastically coupled to the microcrystals since the roughness of the surface is higher when a larger amount of material immobilizes on the gold surface. During the first reduction step, this water is mostly pushed out from the surface layer due to the formation of a new surface structure.

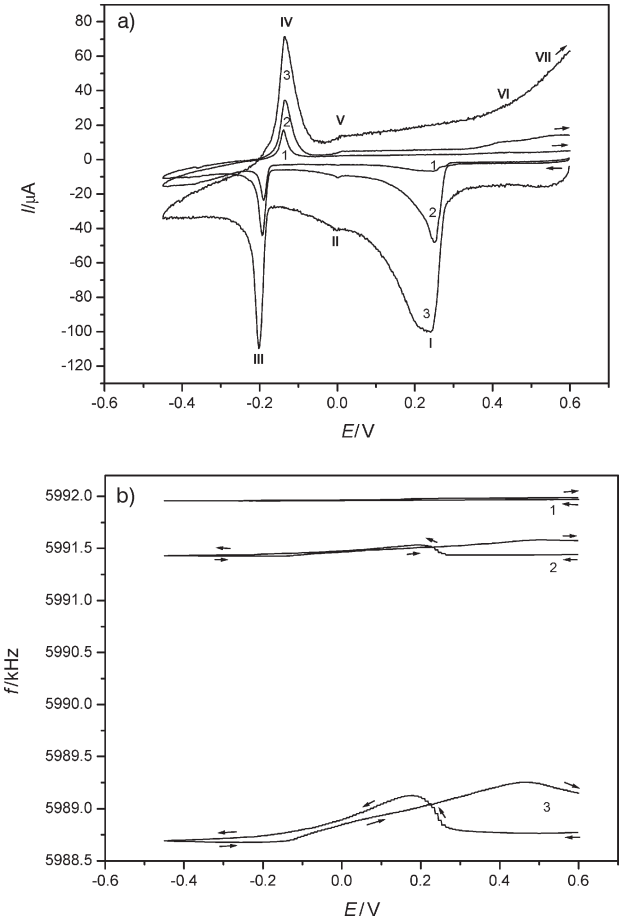

F i g . 3 — *Cyclic voltammograms (a) and the respective EQCM frequency responses (b) obtained for the $RuCl_3$ microcrystals attached to a gold surface in the presence of 0.5 mol dm^{-3} solution of NaCl. The amount of material attached 0.42 μg (1), 6.16 μg (2), and 21.7 μg (3). Scan rate: 20 mV s^{-1}. First cycle.*

Based on the results obtained the following reaction scheme can be given:

(a) For peak I of the first cycle

$$z\,Ru^{III}Cl_3 \cdot (H_2O)_x + n\,e^- + (n-t)\,K^+ \rightarrow K^+_{n-l}[Ru^{III}_{z-n}Ru^{II}_{n}Cl_{3z-t}(H_2O)_y] + (z\,x-y)\,H_2O + t\,Cl^- \quad (2)$$

where $n \geq t$.

With the help of eq. (2), the high mass loss and the larger charge consumed during the very first reduction step can be explained. We may also assume

that chloride ions remain in the layer, but in a different, interstitial position as counter-ions.

During the subsequent reduction steps, further reduction of Ru(III) takes place, which involves the incorporation of cations and water molecules (waves II–IV). The amount of the water sorbed depends on the hydration of the cations. Structural changes also occur.

Therefore, the further reversible redox processes occurring at waves IV–V, III–VI and II–VII in the presence of K^+ ions, or III–IV, II–V in the presence of Na^+ and Cs^+ ions may be given as follows:

$$K^+_{n-t}[Ru^{III}_{z-n}Ru^{II}_{n}Cl_{3z-t}(H_2O)_y] + m\,e^- + m\,K^+ + p\,H_2O \rightleftarrows K^+_{n+m-t}[Ru^{III}_{z-n+m}Ru^{II}_{n+m}Cl_{3z-t}(H_2O)_y]\cdot p\,H_2O \quad (3)$$

which occur in more steps.

The 'complete' reoxidation at waves labeled VI and/or VII, or VIII and IX, i.e., those appearing in the potential region ca. 0.4 V – 0.7 V, depending on the nature of the cations during reoxidation, may be assigned to the following reaction:

$$K^+_{n-t}[Ru^{III}_{z-n}Ru^{II}_{n}Cl_{3z-t}(H_2O)_y]\cdot d\,H_2O \rightleftarrows K^+_{n-t-q}[Ru^{III}_{z-n+q}Ru^{II}_{n-q}Cl_{3z-t}(H_2O)_y]\cdot c\,H_2O + q\,e^- + q\,K^+ + b\,H_2O \quad (4)$$

During subsequent cycles, this oxidized form will be reduced in several steps, and reoxidation will take place according to the scheme given above. That means that the original $zRu^{III}Cl_3\cdot(H_2O)_x$ form is irreversibly converted to this oxidized form.

The rather high frequency increase cannot be explained solely by the mass loss related to the amount of water molecules (crystal water) and chloride ions leaving the surface layer, especially because a mass increase should also be assumed due to the incorporation of cations. It is most likely that the large frequency increase is partly related to the strain and stress arising from the structural changes (phase transition) of the surface layer.

Tetracyanoquinodimethane

Although the dissolution does not entirely prevent the analysis of the immobilized microcrystals, it is desirable to diminish the solubility to the highest possible degree. One of the possible strategies is the decrease of the solvent activity and the solubility product by application of supporting electrolytes of high concentration. The idea was tested on TCNQ microcrystals by using LiCl solutions. LiCl is highly soluble in water and decreases water activity to a high degree.

In dilute LiCl solutions, a gradual dissolution of the immobilized TCNQ microcrystals may be observed in the potential region where $TCNQ^{\cdot-}$ anion radicals are formed. Because not all the TCNQ sites of the microcrystals are reduced during potential cycling (the extent of reduction depends on the scan rate, v), the following reaction may be written:

$$x\,TCNQ + y\,e^- + y\,Li^+ \rightleftarrows (TCNQ)_{x-y}(TCNQ^{\cdot-})_y(Li^+)_y \quad (5)$$

Fig. 4 shows the first two cyclic voltammograms and the corresponding EQCM frequency curves obtained for a freshly prepared TCNQ layer. During the first reduction cycle a small wave (I) develops at −0.12 V, which is accompanied by a mass increase; however, this wave disappears later.

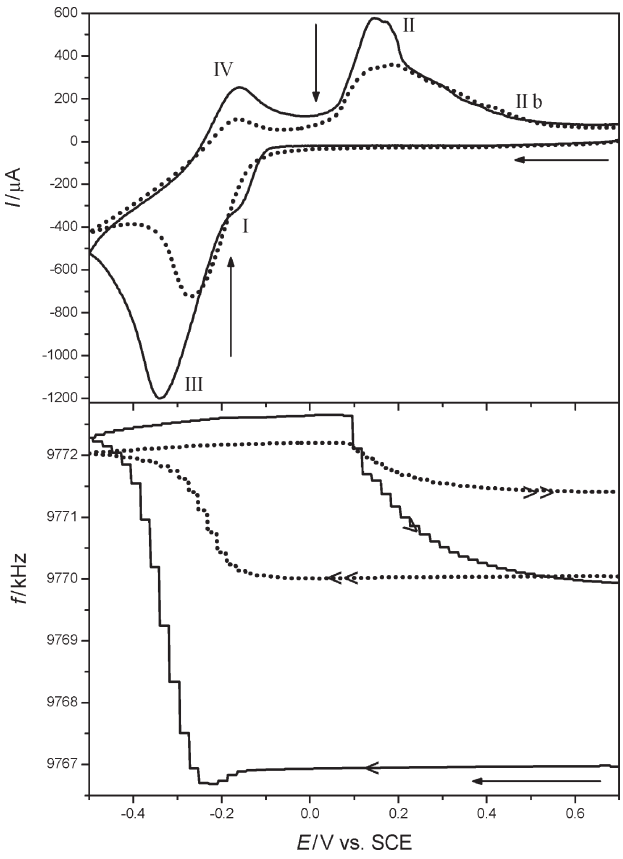

Fig. 4 – *Cyclic voltammograms (upper curves) and the simultaneously detected EQCM frequency changes (lower curves) for TCNQ microcrystals freshly deposited on gold in contact with 0.5 mol dm^{-3} LiCl solution. Scan rate: 50 mV s^{-1}. First cycle (——), second cycle (·····).*

The dissolution starts at the foot of the large reduction wave III (frequency increase), the extent of dissolution is proportional to the charge injected, and the dissolution continues until a negative current flows after the scan reversal. An interesting feature of the frequency excursion is that during reoxidation a frequency decrease may be observed,

indicating the redeposition of the dissolved TCNQ. The precipitation continues at + 0.5 V as indicated by the frequency decrease during the waiting time at 0.5 V.

The expected frequency change due to the incorporation of Li^+ ions (and water molecules) is suppressed by the frequency change caused by extensive dissolution, as the reprecipitation also overcomes the mass decrease related to the desorption of the charge compensating Li^+ ions.

The dissolution manifests itself also in the gradual decrease of the peak currents (charge consumed). The wide 'inert zone', i.e., large separation of the reduction and reoxidation peaks typical of solid-solid phase transformation under rate control by nucleation and growth may also be seen in the cyclic voltammograms displayed in Fig. 4.

The main reduction wave (III) appears at a more negative potential, and the peak potential, E_{pc} (III), shifts into the direction of more positive potentials during subsequent cycles. During the first cycles, counterions and solvent molecules enter the layer, making further transport processes easier, consequently the overpotential related to the hindered transport processes, e.g., diffusion of ions decreases. In the case of TCNQ microcrystals it was also assumed that during the initial redox cycling, a change occurred in the morphology, crystalline state of the material attached.[25]

The prewave (I) may be explained by the reduction of the TCNQ molecules that results in the formation of $Li^+TCNQ^{\cdot-}$. The appearance of peak III and peak IV is most likely in connection with the formation and reoxidation of $TCNQ^{2-}$ dianion in the part of the layer that was dissolved but remained near the gold surface in the form of a solution saturated with reduced TCNQ species.

Due to the immiscibility of the phases, the first one-electron reduction wave of TCNQ shifts into the direction of more negative potentials; however, in this potential region in the solution, further reduction of $TCNQ^{\cdot-}$ may take place:

$$TCNQ^{\cdot-}Li^+ + e^- + Li^+ \rightleftarrows TCNQ^{2-}Li_2^+ \qquad (6)$$

These explanations are supported by the fact that when no dissolution of $Li^+TCNQ^{\cdot-}$ takes place, i.e., in concentrated LiCl solutions (see later), the formation of $Li_2^+TCNQ^{2-}$ occurs at more negative potentials, although an opposite shift of the peak potential would be expected due to the effect of the concentration (activity) of the Li^+ ions.

There is another oxidation 'postwave' (IIb), which is also associated with the dissolution, and may be assigned to the reoxidation and redeposition of the dissolved $TCNQ^{\cdot-}$ ions, which diffuse back to the gold surface. It was observed that during cycling, peak IIb grows at the expense of wave II.

Dissolution may also be observed at more concentrated LiCl solutions; however, the rate of dissolution decreases. There is no dissolution at concentrations higher than 12 mol dm^{-3} which indicates that the decrease in water activity plays a critical role (c_{LiCl} = 0.5 mol kg^{-1}, a_{H_2O} = 0.98; c_{LiCl} = 18 mol kg^{-1}, a_{H_2O} = 0.21;[40]).

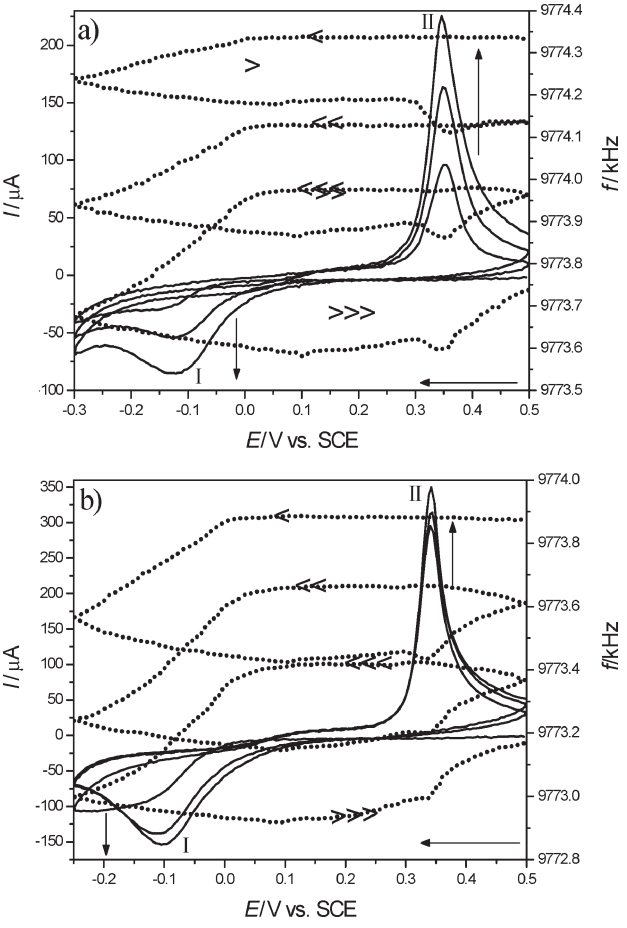

Fig. 5 – *Cyclic voltammograms (——) and the EQCM responses (·····) for TCNQ microcrystals freshly deposited on gold in contact with 12 mol dm^{-3} LiCl solution. Scan rate: 20 mV s^{-1}. (a) first three cycles, (b) cycles from 4th to 6th.*

Fig. 5a shows the first three cycles obtained for a freshly deposited layer. Contrary to that observed in dilute solutions, the voltammetric current continuously increases and the frequency decreases during subsequent cycles. Practically no frequency change occurs until the first reduction wave, when only a small capacitive current flows. Simultaneously with the reduction process, a mass increase may be observed, which is expected since counterions should enter the layer in order to maintain the electroneutrality. At the end of each cycle, the frequency is smaller than the initial one. It is a typical break-in pattern[41] indicating that solvent

molecules and possibly salt remain in the layer. During the break-in period, a rather unusual variation of frequency is observable during reoxidation at wave II. Instead of a frequency increase – since the charge-compensating cations should leave the surface layer – first a frequency decrease takes place, and the frequency starts to increase only after the voltammetric peak.

This phenomenon gradually ends, and the expected mass decrease becomes dominant. It may be explained by the incorporation of anions in the course of the first cycles. The effect observed is kinetic in nature, i.e., instead of desorption of cations, the sorption of anions takes place in order to compensate the excess positive charge of the cations inside the layer when TCNQ sites are reoxidized and become neutral. Because, for a broken-in film, we measure almost equilibrium mass changes as a function of the charge consumed, as well as knowing the amount of the material on the gold surface and the mass increase after the break-in period we can make some estimation in this respect (see later).

In order to complete the break-in, many potential cycles were executed. In order to illustrate the characteristic changes we have also presented cycles 4 to 6 (Fig. 5b). It should be mentioned that there is also a secondary break-in or waiting time effect, i.e., the frequency increases when the potential of the electrode is held at + 0.5 V. This means that during the perfect reoxidation, which is possibly accompanied by structural changes, the ions and solvent molecules leave the film. During the break-in period, the frequency does not regain its initial value.

No dissolution may be observed even at rather low scan rates. Fig. 6 shows the voltammetric and EQCM responses at 1 mV s^{-1} for a broken-in layer.

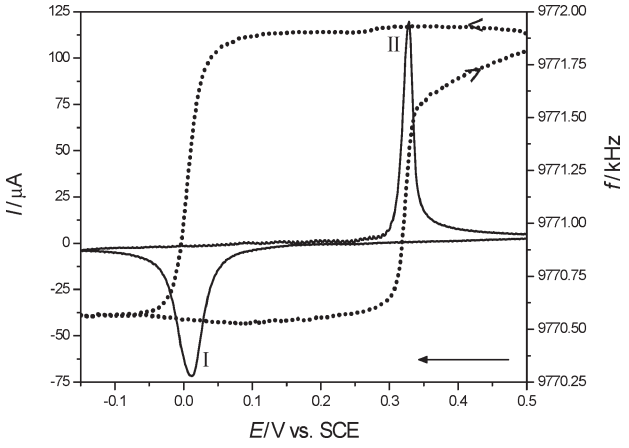

F i g . 6 – *Cyclic voltammograms (——) and the EQCM frequency response (·····) of the TCNQ microcrystals after the break-in period shown in Fig. 5, in the same concentrated LiCl solution. Scan rate: 1 mV* s^{-1}.

Based on the data presented in Fig. 6 the apparent molar mass calculated by using eq. (1) was found to be M_{app} = 55 ± 5 (for the reduction) and M_{app} = 60 ± 5 (for the oxidation).

These findings indicate that solvent molecules enter together with Li^+ ions in the surface TCNQ layer during the reduction, and the amount of solvent molecules sorbed during the reduction depends on the initial state. When the TCNQ layer is fully reoxidized, the solvent molecules and the LiCl salt leave the layer rather slowly. It is also instructive to calculate the amount of the conversion of TCNQ sites. The total amount of TCNQ on the gold surface was determined from the frequency difference measured for the coated and uncoated crystals, respectively, in dry state. This was re-checked by complete dissolution of the layer at the end of the investigations. For instance, for the layer investigated in the experiments shown in Figs. 4 and 5, the dry mass on the surface was 40 μg (22 kHz), which means a surface coverage $\Gamma = 4.85 \cdot 10^{-7}$ mol TCNQ cm^{-2}. After the break-in, the total mass change of the layer was found to be ca. 5 μg (2.5 kHz). It follows that under these conditions $7 \cdot 10^{-7}$ mol H_2O cm^{-2} or $4.75 \cdot 10^{-7}$ mol LiCl cm^{-2} remained permanently in the surface layer. We cannot distinguish between neutral species; however, it is evident that after the break-in, the microcrystals contain neutral, low molar-mass entities the amount of which is comparable to that of the TCNQ in the surface layer. During a single cycle (Fig. 6) Q = 3.8 mC was consumed, indicating that $4 \cdot 10^{-8}$ mol TCNQ was reduced, i.e., only ca. 20 % of the TCNQ molecules were involved in the electrochemical transformations even at rather low (1 mV s^{-1}) scan rate.

Fig. 7 shows the chronoamperometric-microgravimetric responses during a reduction potential step. After the vertical spike associated with the onset and decay of the capacitive charging current, a peaked current-time transient developed. The latter is proof for the existence of nucleation and growth kinetics.[16] Such behaviour is expected, since the cyclic voltammograms also show the diagnostic criteria of the solid-solid phase transformation (large separation of the reduction and oxidation peaks, narrow peak widths). In contrast to that observed in the case of the reduction of phenazine microcrystals (see later),[33] the EQCM response does not reflect the phase transition; the frequency decrease is continuous, indicating the unhindered sorption of Li^+ ions together with water molecules of their hydrate sphere.

From chronoamperometric – EQCM data shown in Fig. 7, M_{app} = 48 ± 8 g mol^{-1} may be calculated which is in good accordance with that derived from the cyclic voltammetric – EQCM experiments. Somewhat surprisingly for the reoxidation,

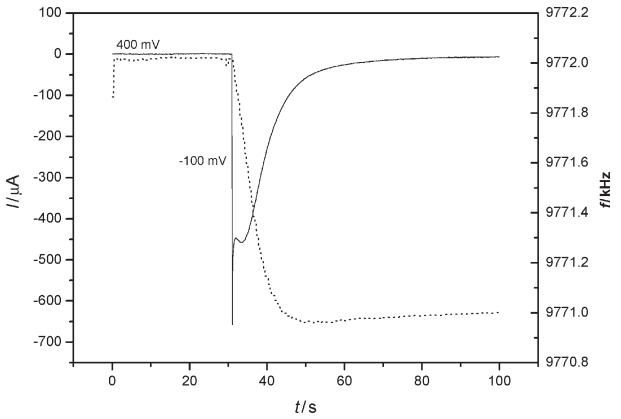

F i g . 7 – *Chronoamperometric response (——) and the simultaneously obtained EQCM frequency changes (·····) for the reduction of TCNQ microcrystals immobilized on gold in contact with 12 mol dm^{-3} LiCl solutions. The potential was stepped from 400 mV to –100 mV. (a) 0 – 100 s, (b) 0 – 45 s (enlarged).*

a substantially higher value, M_{app} = 155 ± 15 g mol^{-1}, may be derived when small-amplitude potential steps are applied in the potential region where the reoxidation starts (Fig. 7). This might be in connection with the strain effect and/or the phase transition is accompanied with a fast dehydration.

Phenazine

Phenazine and its derivatives have been studied extensively due to interesting chemical, biochemical, electrochemical and photochemical reactions of these compounds.[33] Phenazine is practically insoluble in water; however, it can be dissolved in organic solvents or in concentrated aqueous solutions of acids.

Fig. 8 shows the break-in effect observed for phenazine microcrystals attached to gold. As seen, a substantial amount of electrolyte is gradually incorporated into the surface layer together with increasing charge consumed (Q) during subsequent cycles. The mass increase attributable to sorption of ions and solvent molecules starts simultaneously with the first reduction step (peak I) and continues – albeit in a smaller rate – in the region of peak II, and even during reoxidation (peak III). The mass decrease begins at the second oxidation wave (peak IV); however, at the end of the cycles a considerable amount of electrolyte remains embedded in the surface layer. The difference between the initial and final mass (frequency) values decreases with the number of cycles and eventually reaches a more or less constant value. It should be mentioned that the oxidation is incomplete after the end of the cycle, $Q_{red} > Q_{ox}$, and a small current accompanied with a slight frequency increase still flows for several minutes. Consequently, the next cycle starts at a somewhat higher frequency value depending on the waiting time, although no dissolution of microcrystals

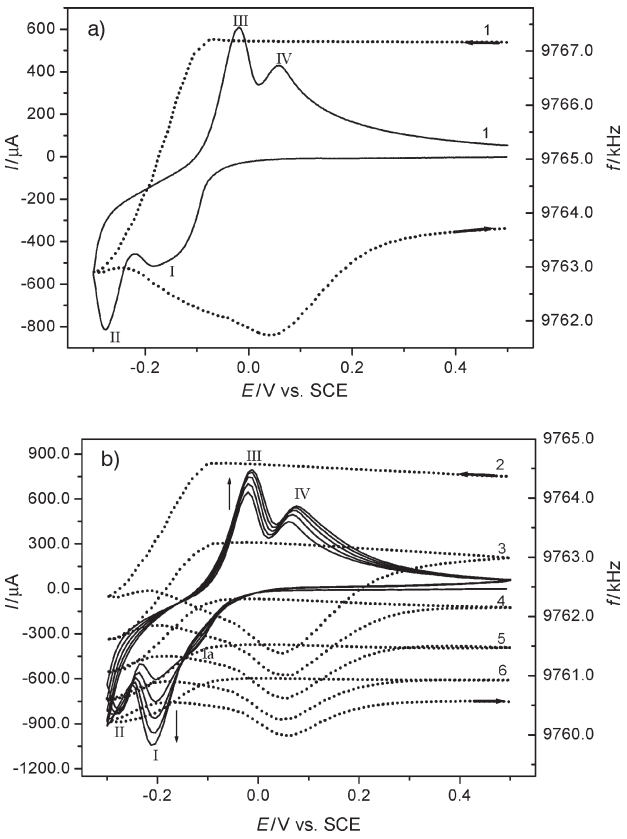

F i g . 8 – *Consecutive cyclic voltammograms (——) and the simultaneously detected EQCM frequency responses (·····) for phenazine microcrystals attached to a gold electrode in the presence of 1 mol dm^{-3} HCl/NaCl (pH 2) solution. Scan rate: 50 mV s^{-1}. (a) First cycle for the freshly prepared layer. Dry thickness is ca. 50 μm. (b) Cycles 2 – 6, the second cycle was taken after 1 min waiting time at 0.5 V.*

occurs. This is best seen by comparing the final frequency value after the first cycle in Fig. 8a and the starting frequency of the second cycle (Fig. 8b) after 1 min waiting time at 0.5 V. During continuous cycling, the positions of the peaks do not change substantially. The number and the variation of the peaks indicate a complex mechanism, the formation and transformation of several reduction intermediate products, and the reoxidation of those species.

The phenazine at pH 2 – since pK_a = 1.23 – exists in both unprotonated (P) and protonated forms (PH^+) at equilibrium. Therefore, the first electron transfer may be described as follows:

$$P + e^- + H^+ \rightleftarrows PH^\bullet \quad (7)$$

$$PH^+X^- + e^- \rightleftarrows PH^\bullet + X^- \quad (8)$$

$$PH^\bullet + H^+ + X^- \rightleftarrows PH_2^{\ddagger\bullet}\ X^- \quad (9)$$

$$P + e^- + 2\ H^+ + X^- \rightleftarrows PH_2^{\ddagger\bullet}\ X^- \quad (10)$$

where $PH^\bullet$ and $PH_2^{\ddagger\bullet}$ are phenazyl radical and phenazylium radical cation, respectively.

The events at peak II are more complicated. We assume the reduction of $PH_2^{+\bullet}$ and the formation of 5,10-dihydrophenazine (PH_2) which may also be protonated in strong acid solutions (PH_3^+):

$$PH_2^{+\bullet}\ X^- + e^- \rightleftarrows PH_2 + X^- \qquad (11)$$

$$PH_2^{+\bullet}\ X^- + e^- + H^+ \rightleftarrows PH_3^+X^- \qquad (12)$$

Reaction (11) is most likely at pH 2, and it is in accordance with the small frequency increase or at least the substantial decrease of the slope of frequency-potential curves in this potential region. Because H^+ ions do not participate in reaction (11) and reaction (12) proceeds only to a certain extent in very acidic media, the much smaller pH-dependence of the peak potential becomes understandable. However, unreacted phenazine is still present in high concentration in the adjoining layer. Therefore, the formation of phenazinehydrine charge-transfer complex is preferred:[42]

$$P + PH_2 \rightleftarrows P\text{-}PH_2 \qquad (13)$$

The blue colour of this complex may be seen. The composition of the charge-transfer complex may be varied. Therefore, the formulas of the complexes may be given as follows: $(P)_x(PH_2)_y(H_2O)_z$, $(P)_x(PH_2^{+\bullet})_q(X^-)_q(H_2O)_z$ or $(PH_2^{+\bullet})_q(PH_2)_y(X^-)_q(H_2O)_z$. The charged complexes may be formed by the reaction between P and $PH_2^{+\bullet}\ X^-$ or in the course of further reduction of $P–PH_2$, i.e.,

$$P–PH_2 + e^- + 2\ H^+ + X^- \rightleftarrows PH_2^{+\bullet}\ PH_2X^- \qquad (14)$$

This explains the further mass increase after the sweep reversal until $I < 0$. However, all these changes depend on the experimental time scale. Reaction (13) is a chemical reaction the rate of which may be limited either by the rate of the chemical reaction or by the diffusion. This is the very reason for the potential independent and/or currentless mass changes observed during potentiostatic experiments. The most surprising effect was that after a slight mass decrease at the foot of peak III, a rather large mass increase could be observed. The uptake of further anions is connected with the oxidation of the reduced phenazine. Two types of species are present: the charge-transfer (CT) complexes of different compositions and 5,10-dihydrophenazine. Reaction (11) proceeds in the reverse direction in this potential region and the oxidation of CT complexes may be described as follows:

$$P–PH_2 + X^- \rightleftarrows P–PH_2^{+\bullet}\ X^- + e^- \qquad (15)$$

$$PH_2^{+\bullet}\ PH_2X^- + X^- \rightleftarrows (PH_2^{+\bullet})_2(X^-)_2 \rightleftarrows 2\ PH_2^{+\bullet}\ X^- + e^- \qquad (16)$$

This explains the mass increase observed since these reactions result in the formation of additional, positively charged ions and the charge compensation involves the sorption of anions. The maximum mass increase is achieved in the region of peak IV which may be related to the formation of unstable $PH_2^{2+}(X^-)_2$ species during further oxidation:

$$PH_2^{+\bullet}\ X^- + X^- \rightarrow PH_2^{2+}(X^-)_2 + e^- \qquad (17)$$

It is instructive to compare the total amount of phenazine on the surface with the amount of sorbed water molecules. The deposition of the phenazine caused a frequency change $\Delta f = -10200$ Hz in dry state. It is equivalent to $2.19 \cdot 10^{-7}$ mol phenazine on the gold surface. No swelling or dissolution was observed upon immersing the electrode into water or acid solutions since $\Delta f = -(4800 \pm 400)$ Hz frequency decrease was observed for both the uncoated and the coated gold crystals. It follows that during the initial cycle at peak I only 8 % of phenazine was reduced since $1.6 \cdot 10^{-8}$ mol Cl^- entered the layer, however, 4.2 mol H_2O/1 mol phenazine sorbed in the layer. The latter ratio is 54 if we consider only the "active" part of phenazine crystals. The amount of embedded water at the end of the cycle is $7.59 \cdot 10^{-7}$ mol H_2O (or H_2O equivalent electrolyte) or taking into account the desorption (relaxation) at +0.5 V this value becomes $6.72 \cdot 10^{-7}$ mol H_2O, i.e. the permanent residue after the first cycle is ca. 3 mol H_2O/1 mol phenazine. At the end of the 6 cycles, the total swelling is ca. 7 mol H_2O/1 mol Ph, while 12 % of the phenazine became active.

The results of potential step – potentiostatic experiments reveal that beside the potential-induced fast and large mass changes associated with electron transfer reactions accompanied with the sorption/desorption of ions and water molecules, there are also slow mass changes that are almost independent of the potential, and continue for a long time while only a very small or no current flows. This indicates a slow diffusion inside the layer and chemical reactions. There are dominant mass changes: mass increase during reduction in the potential interval from 0 V to –0.1 V (peak I on the cyclic voltammogram) and mass decrease with the same magnitude that starts at ca. 0.1 V that corresponds to peak IV. An important feature appears when the potential was stepped from –0.1 V to –0.2 V (Fig. 9). After the vertical spike, which is connected with the rapid onset and decay of the capacitive charging current, a peaked current-time transient develops. The latter is proof for the existence of nucleation and growth kinetics. With this observation we have all the diagnostic criteria for solid-solid phase transformation under the rate control of nucleation and growth, since the other characteristic features (large separation of the reduction and oxidation peaks, narrow peak widths, and the

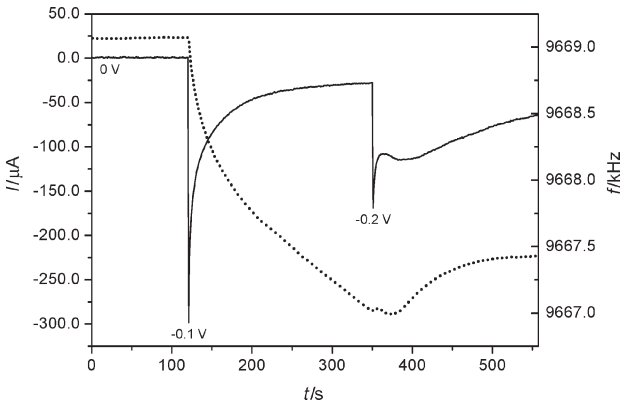

F i g . 9 – *Successive potential steps from 0 V to –0.1 V and then to –0.2 V. Experimental conditions are described in Fig. 8. Note the peaked current-time transient after stepping from –0.1 V to –0.2 V.*

typical scan rate dependence when the peaks at lower scan rates emerge from the rising portion of the voltammograms)[16] may be seen on the cyclic voltammograms. However, we can add a new characteristic to those theoretically established in the literature. A closer inspection of the frequency response presented in Fig. 9 reveals a characteristic pattern, frequency increase/decrease in the region of phase transformation.

Electropolymerization of carbazole

Fig. 10 shows the first cycle and the simultaneously obtained frequency changes for a rather thin, virgin carbazole film on gold deposited by evaporation technique. (For the sake of comparison, the background responses are also presented.)

The amount of the carbazole on the surface and thickness of this film were estimated from the frequency measured before and after deposition of the material. The measured value, –1341 Hz corresponds to ca. 2.5 μg, i.e. to a surface coverage: $3.75 \cdot 10^{-8}$ mol cm^{-2}. The results shown in Fig. 10 obtained for a thin film are very instructive because in this case the total amount of carbazole sample on the surface was oxidized during a single cycle. As seen in Fig. 11, displaying the next two cycles, the high oxidation peak did not appear, only the reversible redox response of the polymer may be observed. From these data, we are able to calculate the mass changes accompanying the dimerization (polymerization) process and the redox transformations, respectively. In the course of the first irreversible oxidation of the carbazole sample, a –670 Hz frequency decrease could be detected and the total charge consumed for the oxidation was 1.778 mC. By using the Sauerbrey equation Δm = 1.26 μg the surface mass change can be calculated. The amount of the incorporated ClO_4^- ions may be estimated from the charge consumed. The number of electrons involved in the oxidation of a carbazole molecule and that of the dimer formed, n = 3. However, for the electropolymerization usually n = 2.5 is considered, i.e., two electrons are associated with the polymerization and 0.5 electrons are associated with doping one monomer unit in PCz.[31] This means that the primary oxidation wave is a mixture of ECE and EC processes and a single charge is distributed for every two monomer units in a reasonably long polycarbazole chain. By using n = 2.5, the sorption/desorption of $7.4 \cdot 10^{-9}$ mol ClO_4^- ions may be calculated, which corresponds to a mass change of 0.74 μg. Considering also the slight mass loss due to the desorption of H^+ ions during the dimerization process, a surplus of 0.52 μg (1.26 – 0.74) remains. This amount could be assigned to the sorption of solvent molecules, consequently ca. $2.9 \cdot 10^{-8}$ mol H_2O molecules, i.e., 4 H_2O molecules per 1 ClO_4^- ion also enter the film during the oxidation process. A comparison with the mass of carbazole on the surface reveals that indeed only one half of carbazole dimers are oxidized to a dication form since the total amount of carbazole on the surface was $1.5 \cdot 10^{-8}$ mol, while the number of the positively charged sites was found to be $7.4 \cdot 10^{-9}$ mol.

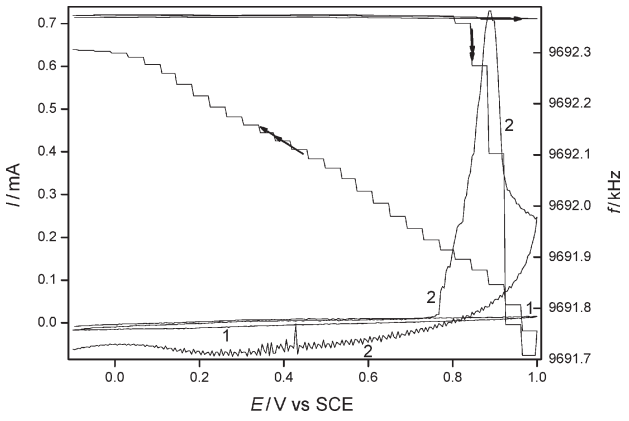

F i g . 1 0 – *The cyclic voltammetric curves and the simultaneously detected frequency changes obtained for the gold substrate (1) and the virgin carbazole layer deposited on a gold electrode (2), respectively. Solution: 9 mol dm^{-3} $HClO_4$. Scan rate: 50 mV s^{-1}.*

Redox transformations of polycarbazole

Fig. 11 shows the next two cycles which curves already exhibit typical responses of polycarbazole films.[12,19] The difference between the first and the subsequent cycles relates to a secondary break – in effect. (The first cycle in Fig. 11 was taken after 1 min delay time at –0.1 V.)

The redox transformations are accompanied with a mass increase during oxidation and a mass decrease during reduction. However, a closer in-

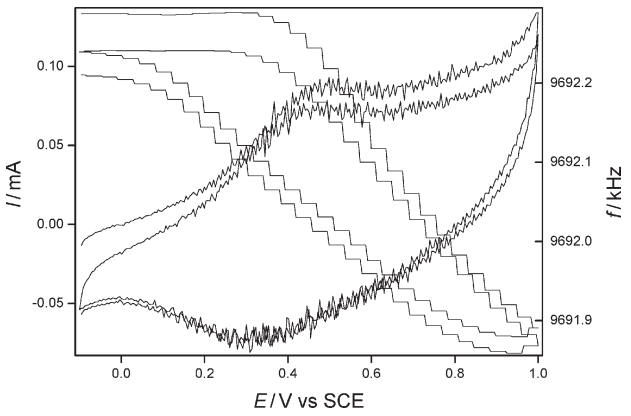

F i g . 11– *Continuation of the experiment shown in Fig. 10, the 2nd and the 3rd cycles*

spection of the frequency responses reveals that in fact three sections could be distinguished. Similar to the redox transformation of polyaniline,[41] the current begins to increase, i.e., a certain amount of charge is injected, prior to the frequency decrease (mass increase). Therefore, it may be assumed that in the first stage of oxidation, deprotonation occurs and the protons leave the film. Owing to the very low molar mass of hydrogen ions, only a very small mass decrease (providing that H^+ ions and not H_3O^+ ions cross the film/solution interface) could be expected. The second section belongs to the first redox process while the third one to the further oxidation. There is no substantial difference in the slopes of the frequency – potential or frequency – charge plots with respect to these two oxidation steps, although these slopes of the second oxidation process are somewhat smaller. From the slope of $\Delta m - Q$ plots an equivalent (apparent) molar mass (M) for the mobile species causing the mass changes may be calculated. If the formation of one positively charged site is expected as a result of a $-1e^-$ oxidation process, one ClO_4^- ion has to enter the film in order to maintain the electroneutrality. In this case $M = 99.5$ g mol^{-1} may be calculated. However, the calculation by using the respective data derived from the experiments shown in Fig. 11 gives a value of $M = 61$. This means that – if the silent H^+ ion transport is neglected – the sorption of ClO_4^- ions is accompanied by the desorption of water molecules since no other reversible processes can be assumed. Quantitatively, while one ClO_4^- ion enters the film, more than two water molecules leave the surface layer.

Conclusions

It has been demonstrated that microcrystals can be attached firmly to gold surfaces and be investigated in aqueous solutions by electrochemical techniques without the dissolution of the immobilized samples. It has also been proven that there is no loss of material due to vibration of the oscillating quartz crystal. When the product of the electrochemical reaction that is a charged species is soluble in water, the dissolution may be prevented by decreasing the water activity of the contacting solution as presented for TCNQ crystals. The results of the cyclic voltammetric and potential step quartz crystal nanobalance experiments attest that rather complicated events occur during the electrochemical transformations of the microcrystals that involve changes of the surface mass due to the sorption/desorption of ionic species and solvent molecules. The first cycles always differ from the subsequent ones; however, the reason is usually different. In the case of phenazine, a usual break-in pattern appears, i.e., a gradual increase of the electrochemical activity and the swelling of the surface layer due to the incorporation of solvent molecules and ions. Although the reaction scheme is not simple and formation of charge transfer complexes take place, the changes are reversible. Similar results were obtained for TCNQ crystals. The behaviour of $RuCl_3$ microcrystals is, however, different since during the first reduction step, a new complex compound forms, and the original state cannot be regained during the oxidation. From the second cycle, reversible voltammetric and gravimetric responses may be obtained, which reflect the transformation of the compound formed during the very first cycle. The results presented herein for the electrooxidation of carbazole microcrystals show another case when electropolymerization occurs during the first cycle, and the subsequent EQCM responses are related to the electrochemically active polymer layer formed on the surface. Because of the different crystal structures of the parent compound and its reduction products (see phenazine, TCNQ, $RuCl_3$), solid-solid phase transformations occur during the reduction and the subsequent re-oxidation. The rates of these processes were determined by nucleation/growth kinetics. The evidence for the nucleation mechanism have been found in response functions of both the cyclic voltammetric and potential step experiments, however, it affects also the EQCM frequency response due to the strain in the surface layer. Also demonstrated was that the phase transition proceeds with the release of hydration water.

ACKNOWLEDGEMENTS

Financial supports by the Croatian-Hungarian Research Co-operation Program (CRO-02/2006) and the National Scientific Research Fund (OTKA K71771) is gratefully acknowledged.

References

1. *Scholz, F., Meyer, B.,* Voltammetry of solid microparticles immobilized on electrode surfaces. In: *Bard, A. J., Rubinstein, I.* (Eds.) Electroanalytical Chemistry, vol. 20. Dekker, New York, 1998, p. 1–86.
2. *Fiedler, D. A., Scholz, F.,* Electrochemical Studies of Solid Compounds and Materials In: *Scholz, F.* (Ed.) Electroanalytical Methods Ch. II. 8 Springer, Berlin Heidelberg New York, 2002, pp. 201–222.
3. *Grygar, T., Marken, F., Schröder, U., Scholz, F.,* Coll. Czech Chem. Commun. **67** (2002**)** 163.
4. *Scholz, F., Schröder, U., Gulaboski, R.,* Electrochemistry of Immobilized Particles and Droplets, Springer, 2005.
5. *Scholz, F., Nitschke, L., Henrion, G.,* Naturwissenschaften **76** (1989) 71.
6. *Scholz, F., Nitschke, L., Henrion, G., Damaschun, F.,* Naturwissenschaften **76** (1989) 167.
7. *Lovric, M., Scholz, F.*, J. Solid State Electrochem. **1** (1997) 108.
8. *Scholz, F., Lovric, M., Stojek, Z.*, J. Solid State Electrochem. **1** (1997) 134.
9. *Lovric, M., Hermes, M., Scholz, F.,* J. Solid State Electrochem. **2** (1998) 401.
10. *Komorsky-Lovric, S., Mirceski, V., Scholz, F.*, Microchim. Acta **132** (1999) 67.
11. *Zhuang, Q. K., Scholz, F., Pragst, F.,* Electrochem. Commun. **1** (1999) 406.
12. *Lovric, M., Scholz, F.,* J. Solid State Electrochem. **3** (1999) 172.
13. *Schröder, U., Oldham, K. B., Myland, J. C., Mahon, P. J., Scholz, F.,* J. Solid State Electrochem. **4** (2000) 314.
14. *Komorsky-Lovric, S., Lovric, M., Scholz, F.,* J. Electroanal. Chem. **508** (2001) 129.
15. *Bond, A. M., Marken, F.,* J. Electroanal. Chem. **372** (1994) 125.
16. *Bond, A. M., Fletcher, S., Marken, F., Shaw, S. J.,* J. Chem. Soc. Faraday Trans. **92** (1996) 3925.
17. *Shaw, S. J., Marken, F., Bond, A. M.,* J. Electroanal. Chem. **404** (1996) 227.
18. *Bond, A. M., Marken, F., Hill, E., Compton, R. G., Hugel, H.,* J. Chem. Soc. Perkin Trans. **2** (1997) 1735.
19. *Bond, A. M., Fletcher, S., Symons, P. G.,* Analyst **123** (1998) 1891.
20. *Keyes, T. E., Foster, R. J., Bond, A. M., Miao, W.,* J. Am. Chem. Soc. **123** (2001) 2877.
21. *Wooster, T. J., Bond, A. M., Honeychurch, M. J.,* Electrochem. Commun. **3** (2001) 746.
22. *Zhang, J., Bond, A. M.*, J. Electroanal. Chem. **574** (2005) 299.
23. *Qu, X., Nafady, A., Mechler, A., Zhang, J., Harris, A. R., O'Mullane, A. P., Martin, L. L., Bond, A. M.*, J. Solid State Electrochem. **12** (2008) 739.
24. *Oyama, M., Webster, R. D., Suárez, M., Marken, F., Compton, R. G.,* J. Phys. Chem. **102** (1998) 6588.
25. *Suárez, M. F., Bond, A. M., Compton, R. G.,* J. Solid State Electrochem. **4** (1999) 24.
26. *Doménech, A., Doménech-Carbó, M. T.,* J. Solid State Electrochem. **10** (2007) 949.
27. *Inzelt, G.,* Electrochim. Acta **45** (2000) 3865.
28. *Gergely, A., Inzelt, G.,* Electrochem. Commun. **3** (2001) 753.
29. *Fehér, K., Inzelt, G.,* Electrochim. Acta **47** (2002) 3551.
30. *Inzelt, G.,* J. Solid State Electrochem. **6** (2002) 265.
31. *Inzelt, G.,* J. Solid State Electrochem. **7** (2003) 503.
32. *Inzelt, G., Puskás, Z.,* Electrochim. Acta **49** (2004) 1969.
33. *Puskás, Z., Inzelt, G.,* J. Solid State Electrochem. **8** (2004) 828.
34. *Inzelt, G., Puskás, Z.*, Electrochem. Commun. **6** (2004) 805.
35. *Inzelt, G., Puskás, Z., Németh, K., Varga, I.*, J. Solid State Electrochem. **9** (2005) 823.
36. *Inzelt, G., Puskás, Z.*, J. Solid State Electrochem. **10** (2006) 125.
37. *Inzelt, G., Németh, K., Róka, A.,* Electrochim. Acta **52** (2007) 4015.
38. *Inzelt, G., Róka, A.*, Electrochim. Acta **53** (2008) 3932.
39. *Sauerbrey, G.,* Z. Phys. **155** (1959) 206.
40. *Blandamer, M. J., Engberts, J. B. F. N., Gleeson, P. T., Reis, J. C. R.*, Chem. Soc. Rev. **34** (2005) 440.
41. *Inzelt, G.*, In: *Bard, A. J.* (Ed.) Electroanalytical Chemistry, vol. 18, Marcel Dekker, New York, 1994, p. 89.
42. *Ramage, G. R., Lundquist, J. K.*, In: *Rodd, E. H.* (Ed.) Chemistry of Carbon Compounds, vol. 6, Part B, Heterocyclic Compounds, Elsevier, Amsterdam, London, 1965, pp. 1374–1386.